Graefes Arch Clin Exp Ophthalmol (2017) 255:1193–1202
DOI 10.1007/s00417-017-3671-4

GLAUCOMA

# Optical coherence tomography angiography vessel density mapping at various retinal layers in healthy and normal tension glaucoma eyes

**Joong Won Shin[1] · Kyung Rim Sung[1] · Ji Yun Lee[1] · Junki Kwon[1] · Mincheol Seong[2]**

Received: 7 November 2016 / Revised: 21 March 2017 / Accepted: 3 April 2017 / Published online: 20 April 2017


**Abstract**
*Purpose* To investigate peripapillary vessel density at various spatial locations and layers in healthy and normal tension glaucoma eyes using optical coherence tomography angiography (OCTA).
*Methods* A commercial OCTA device (AngioPlex; Carl Zeiss Meditec) was used to image microvasculature in a 6 × 6-mm optic disc region. Vessel densities of superficial and deep retinal layers were calculated using an automatic thresholding algorithm. Vessel density maps were plotted by averaging individual angiogram images. The spatial characteristics of vessel densities were analyzed at clock-hour sectors and in five 0.7-mm-thick concentric circles from a diameter of 2.0 to 5.5 mm. Areas under the receiver operating characteristics curves (AUCs) assessed the glaucoma diagnostic ability.
*Results* Vessel density maps of superficial and deep retinal layers were significantly reduced at the 7 and 11 o'clock positions in glaucomatous eyes. In superficial layer, vessel density significantly decreased as the distance from the optic disc margin increased, except in the innermost circle (2.0–2.7-mm). There were significant differences in AUCs of superficial vessel density between innermost circle and the other outer circles. In the deep layer, the innermost circle showed significantly higher vessel density than the outer circles. Vessel density at 7 o'clock showed the best diagnostic performance (AUCs, 0.898 and 0.789) both in the superficial and deep layers. The innermost circle showed eccentric feature compared to the outer circles in terms of spatial characteristics and diagnostic ability.
*Conclusions* Understanding of the spatial characteristics of peripapillary vasculature may be helpful in clinical practice and determining the optimal measurement area of vessel density.

**Keywords** Optical coherence tomography angiography · Glaucoma · Vessel density · Superficial and deep retinal layers

## Introduction

Glaucomatous optic neuropathy is defined as the progressive death of retinal ganglion cells (RGCs), a reduction in their axons, and an accompanying deterioration in visual function. Two separate hypotheses have been advanced to explain the possible pathogenesis of this glaucoma, the ischemic theory and the mechanical theory [1–5]. Radial peripapillary capillary (RPC) networks are the most superficial layer of capillaries and a crucial source of nutrition for RGCs and their axons [6, 7]. The importance of RPCs in glaucoma has been proposed in past studies [8, 9], but has not been studied in detail due to a lack of effective tools to evaluate retinal vasculature [10]. Although fluorescein angiography is broadly used to image the retinal vasculature, only 30% of exams provide clear retinal capillary images [11]. In addition, the deeper retinal capillaries are not visualized in angiography because of the effect of a light scattering known as background choroidal fluorescence [11].

✉ Kyung Rim Sung
sungeye@gmail.com

[1] Department of Ophthalmology, College of Medicine,University of Ulsan, Asan Medical Center, 388-1 Pungnap-2-dong, Songpa-gu, Seoul 138-736, South Korea

[2] Department of Ophthalmology, Hanyang University Guri Hospital, College of Medicine, Hanyang University, Guri, South Korea

The recent advent of optical coherence tomography angiography (OCTA) has allowed fast and noninvasive assessment of microvascular perfusion. OCTA can differentiate and visualize the microvasculature of various retinal layers by exploiting depth information. Recent OCTA studies showed reduced vessel density in the optic disc and peripapillary retina of glaucomatous eyes [12–15]. A decreased vessel density spatially corresponds with damaged retinal nerve fiber layer (RNFL) bundles [16, 17]. However, the spatial characteristics of peripapillary microvasculature were incompletely understood in previous OCTA studies because the area for measuring vessel density was confined to a small region around the optic disc. There is no established consensus for the proper region of vessel density measurement. Moreover, the role of the deep capillary plexus in glaucoma remains unclear. A precise layer-by-layer assessment of the glaucomatous vascular change in conjunction with spatial information would greatly expedite research into the vascular mechanisms of glaucoma.

Hence, we aimed to investigate the characteristics of peripapillary vessel density at various spatial locations and layers in healthy and glaucomatous eyes using commercially available OCTA. The discrimination capability of vessel density between healthy and glaucomatous eyes was also evaluated at various spatial locations and layers. We sought to determine the optimal region for peripapillary vessel density measurement by assessing spatial characteristics and diagnostic ability.

## Methods

This cross-sectional study was performed on healthy and glaucoma individuals who visited the glaucoma clinic of Asan Medical Center, Seoul, Korea, from April 2016 to July 2016. The institutional review board of Asan Medical Center approved this study, and the study design was executed in accordance with the principles of the Declaration of Helsinki. Written informed consent was obtained from healthy subjects before participation, and age-matched data of glaucomatous eyes were consecutively obtained from a medical record review of the relevant period.

### Study subjects

All subjects underwent a comprehensive ophthalmologic examination, including a review of medical history, measurement of best-corrected visual acuity (BCVA), slit-lamp biomicroscopy, Goldmann applanation tonometry, gonioscopy, central corneal thickness assessment (DGH-550; DGH Technology, Inc., Exton, PA, USA), axial length measurement (IOLMaster; Carl Zeiss Meditec, Dublin, CA), fundoscopic examination, stereoscopic optic disc photography, red-free photography, standard automated perimetry (Humphrey Field analyzer with Swedish Interactive Threshold Algorithm standard 24–2 test; Carl Zeiss Meditec), and commercial spectral-domain OCTA (Cirrus HD-OCT 5000 system with AngioPlex OCT angiography; Carl Zeiss Meditec).

To be included, all participants had to meet the following criteria at their initial assessment: a BCVA of 20/40 or better, a spherical refractive error between −6.0 and +3.0 diopters (D), a cylinder correction within +3 D, a normal anterior chamber and open-angle on slit-lamp and gonioscopic examinations, and no history of intraocular pressure (IOP) >21 mmHg. Healthy subjects were included if they had a normal visual field (VF) and a normal appearing optic disc head. In Korea, normal tension glaucoma (NTG) is predominant form of primary open angle glaucoma. Hence, we focused on NTG in current study. NTG subjects, who had no history of IOP >21 mmHg, were included based on the presence of RNFL defects on red-free photography or the presence of glaucomatous optic disc changes on optic disc photography (such as disc hemorrhage or neuroretinal rim notching or thinning) and the presence of VF defects that corresponded with RNFL defects and optic disc changes. A VF defect was defined as: (1) the presence of a cluster of three or more non-edge contiguous points on a pattern deviation plot with a $P$ value of less than 5% (one of which had a $P$ value less than 1%) confirmed by at least two consecutive examinations, (2) a pattern standard deviation with a $P$ value less than 5%, or (3) a glaucoma hemifield test result outside normal limits. Only reliable VF test results (i.e., false-positive errors <15%, false-negative errors <15%, and fixation loss <20%) were included in the analysis. The severity of glaucomatous damage was classified as mild (VF mean deviation [MD] ≥ −6 dB) or moderate-to-advanced (VF MD < −6 dB). Patients with any ophthalmic or neurologic disease known to affect the optic nerve head (ONH) or VF were excluded. When both eyes of a subject were eligible, one eye was selected at random.

### Optical coherence tomography angiography

The commercial AngioPlex OCTA device was used to image the microvasculature around the optic disc. This device operates at a central wavelength of 840 nm and a speed of 68,000 A-scans per second. The optical microangiography-complex (OMAG$^c$) algorithm analyzes the change in complex signal (both intensity and phase changes contained within sequential B-scans performed at the same position) [18, 19] and then generates en face microvascular images in a 6 × 6 mm$^2$ region. The 6 × 6 mm scan pattern is composed of 350 A-scans and 350 B-scans. The vascular images of the superficial and deep layers of the retina are displayed separately. The boundaries of the superficial and deep retinal layer slab are automatically determined: (1) from the internal limiting membrane to the inner plexiform layer, and (2) from

the inner plexiform layer to the outer plexiform layer. AngioPlex incorporates the FastTrac retinal-tracking technology to reduce motion artifacts. All scans were individually reviewed by two investigators (J.W.S. and K.R.S.) for quality evaluation (i.e., signal strength, segmentation error, loss of fixation, or motion artifact), and substandard scans were excluded.

The AngioPlex OCTA system provides an Optic Disc Cube scan protocol for RNFL evaluation. The RNFL thicknesses were measured in the 6 × 6 $mm^2$ optic disc area. A built-in algorithm automatically determined the boundary and center of the optic disc and then calculated the area of the optic disc and the circumpapillary RNFL thickness in a 3.46-mm-diameter circle.

### Vessel density measurement and mapping

Image processing and vessel density measurements were performed by a computer program written using MATLAB software (The MathWorks, Inc., Natick, MA, USA). The automatic thresholding algorithm generated a microvasculature image with 25 levels around the optic disc in a 6 × 6 mm region. To minimize missed microvasculature, the tests were repeated 25 times at different threshold levels in each angiography. If the pixel of interest passed a threshold test, 1 score was added at each time. Vessels were defined as regions with more than 5 scores. Vessel density was calculated by the ratio of the total vessel area to the total area of the region of interest. Peripapillary vessel density was measured at various distances from the optic disc center in five 0.7-mm-thick concentric circular regions from a diameter of 2.0 to 5.5 mm (i.e., Circle 1, 2.0 to 2.7 mm; Circle 2, 2.7 to 3.4 mm; Circle 3, 3.4 to 4.1 mm; Circle 4, 4.1 to 4.8 mm; and Circle 5, 4.8 to 5.5 mm). The spatial characteristics of the vessel density were evaluated at quadrant and clock-hour sectors according to the angular location. The clock-hour sectors were measured in a clockwise direction in right eyes and in a counterclockwise direction in left eyes, with the temporal equator set at 9 o'clock. Given that the vascular network pattern differs according to retinal depth [20], vessel density was separately evaluated in superficial and deep retinal layers. Figure 1 shows the schematic regions of vessel density measurements and microvasculature images in the 25 levels demarcated by the automatic thresholding algorithm. The vessel density maps of the healthy and NTG groups were plotted by averaging the individual angiogram images (Figs. 2 and 3). These maps display the probability of the existence of vascular components in a specific spatial location.

### Statistical analysis

Statistical analyses were performed using commercial software (MedCalc, ver. 14.8.1, Mariakerke, Belgium; SPSS, ver. 20.0, IBM Corp., Armonk, NY, USA). Independent t-tests were used to compare continuous variables between healthy and glaucoma subjects. Categorical variables were compared using the chi-square test. Repeated measures analysis of variance (rANOVA) with Tukey's multiple comparison was performed to compare vessel densities among various spatial locations. The Bonferroni correction was used to counteract the problem of multiple comparisons. To evaluate the glaucoma diagnostic ability of vessel density and RNFL thickness, areas under the receiver operating characteristics curves (AUCs) were calculated. Significant differences between AUCs were assessed using the method described by DeLong et al. [21] Univariate and multivariate regression analyses were performed to determine the clinical factors associated with vessel density in glaucoma subjects. $P$ values of .05 or less were considered statistically significant.

## Results

Forty-two NTG eyes and 51 healthy eyes were included in the final analysis. Because of the unacceptable quality of their OCTA images, 10 eyes were excluded. Table 1 summarizes the demographic and clinical characteristics of participants. The VF MD and average RNFL thickness were significantly different between the normal and glaucoma subjects ($P < .001$). The proportion of early (MD ≥ −6 dB) and moderate-to-advanced (MD < −6 dB) glaucoma was 30:12 (71.4:28.6%). There were no significant differences in age, sex, intraocular pressure, refractive error, axial length, central corneal thickness, and disc area between the two groups (all $P > .05$).

### Spatial analysis of vessel density map in the superficial layer

The vessel density maps showed at a glance the spatial characteristics of peripapillary vessel distribution in healthy and glaucomatous eyes (Figs. 2 and 3). Five concentric circular areas were compared in the superficial and deep retinal layers. In the superficial layer (Fig. 2), the vessel density of healthy and glaucomatous eyes gradually decreased according to the distance from the optic disc margin (from circle 2 to circle 5) in every clock-hour sector (all $P < .001$, rANOVA). The innermost circle in healthy and glaucomatous eyes showed lower superficial vessel density than adjacent outer circles from 7 to 11 o'clock. The superficial vessel density was highest at 7 and 11 o'clock in healthy eyes, whereas these regions showed the largest amounts of vascular loss in glaucomatous eyes.

### Spatial analysis of vessel density map in the deep layer

In the deep layer (Fig. 3), the innermost circle in healthy and glaucomatous eyes showed significantly higher vessel density

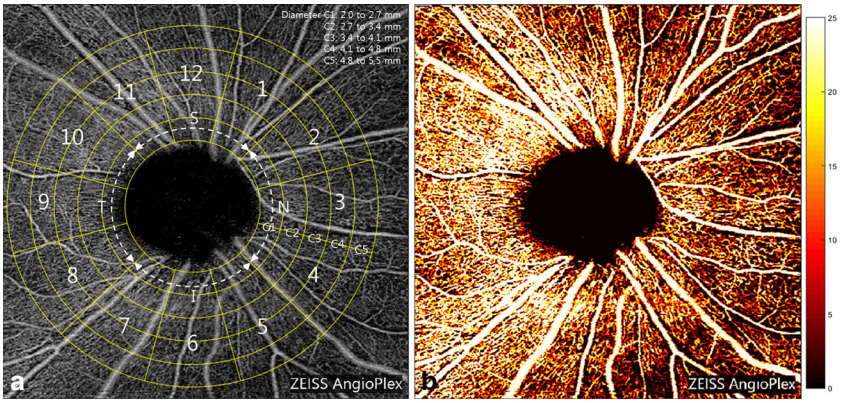


**Fig. 1** Vessel density measurements in optical coherence tomography angiography. (a) Peripapillary vessel density was measured at various distances from the optic disc center in five 0.7-mm-thick concentric circular regions from a diameter of 2.0 to 5.5 mm. Quadrant and clock-hour vessel density was measured according to the angular location. (b) Our automatic thresholding algorithm generated a microvasculature image with 25 levels around the optic disc in a 6 × 6-mm region. The tests were repeated 25 times at different threshold levels in each angiography. If the pixel of interest passed a threshold test, 1 score was added each time. Regions with more than 5 scores were defined as vessels. Vessel density was calculated by the ratio of the total vessel area to the total area of the region of interest. Image processing and vascular density measurements were performed by a computer program written using MATLAB software (The MathWorks, Inc., Natick, MA, USA)

than the outer circles in each clock-hour sector (all $P < .001$). The average deep vessel density of healthy and glaucomatous eyes was not significantly different among circles 3, 4, and 5 (all $P > .05$). In these circles, deep vessel density was highest at 7 o'clock in healthy eyes, followed by 2 and 11 o'clock. Significant deep vascular loss was observed at 7 and 11 o'clock in glaucomatous eyes (all $P < .001$).

Interestingly, deep vessel density was extremely decreased at 12 and 5 o'clock in healthy eyes. In the deep vessel density maps, wedge-shaped vascular insufficiency was observed among relatively rich vascular networks. The deep vessel densities of these areas were not significantly different between healthy and glaucomatous eyes.

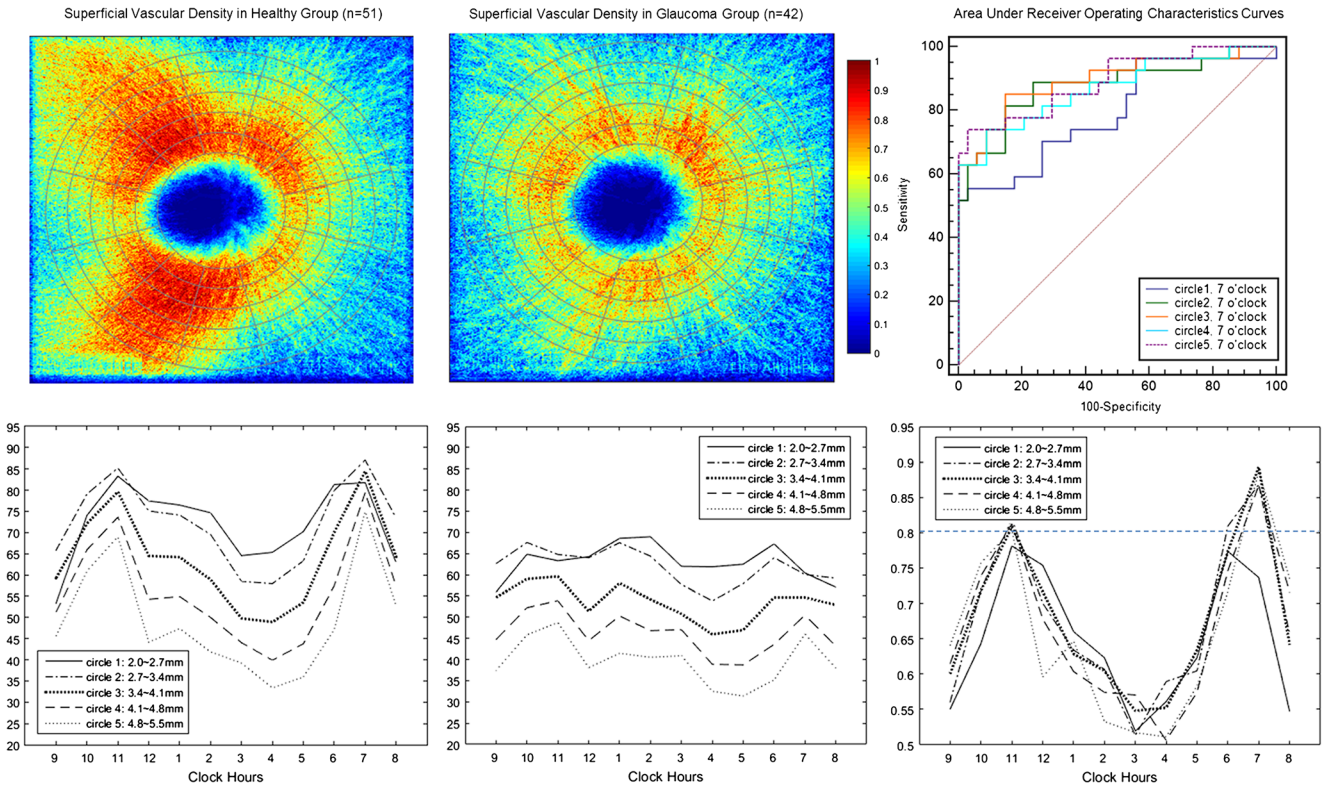


**Fig. 2** Superficial vessel density map in healthy (first column) and glaucomatous (second column) eyes. Area under receiver operator characteristic curves of superficial vessel density for discriminating healthy and glaucomatous eyes (third column)

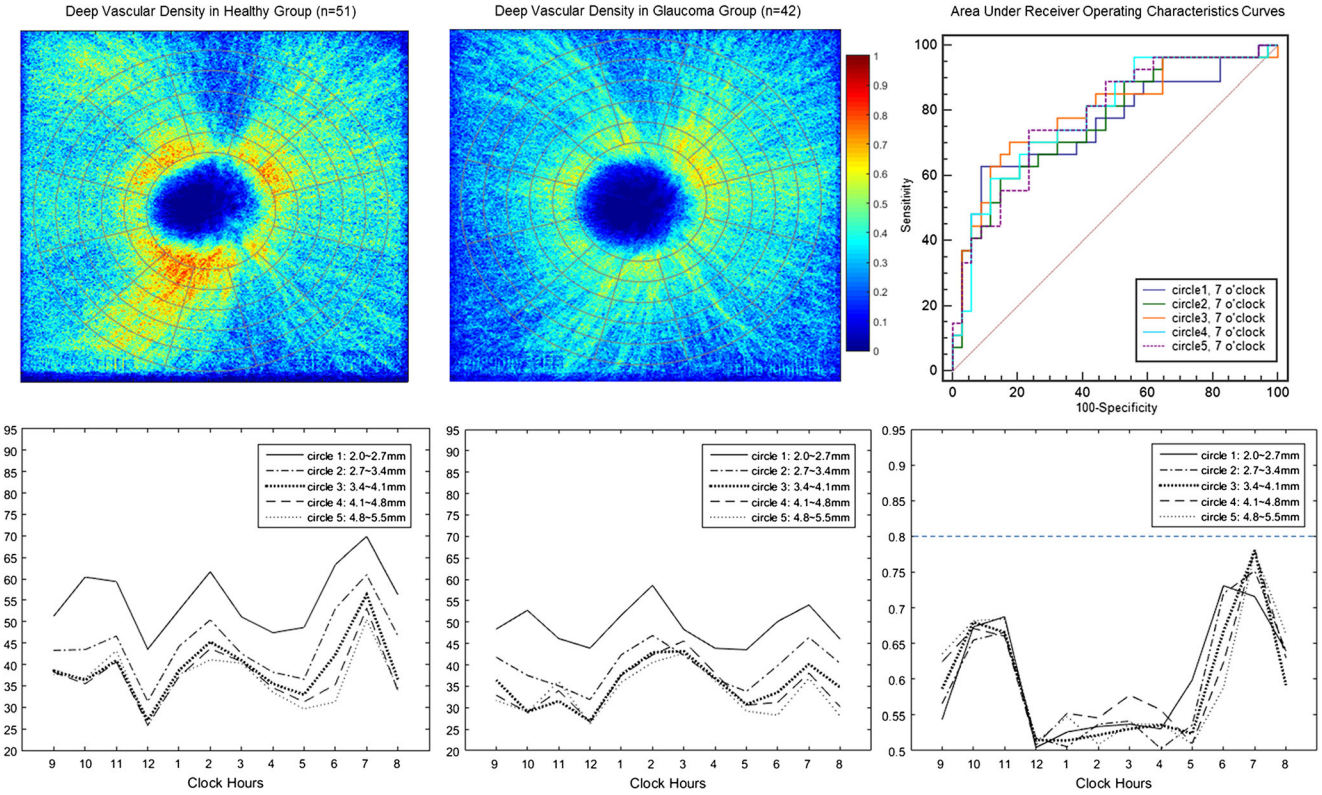


**Fig. 3** Deep vessel density map in healthy (first column) and glaucomatous (second column) eyes. Area under receiver operator characteristic curves of deep vessel density for discriminating healthy and glaucomatous eyes (third column)

### Diagnostic ability of vessel density

The AUCs of vessel density in various locations and layers are presented in Figs. 2 and 3. Circle 3 in the superficial layer showed the best diagnostic performance at 7 o'clock (sensitivity, 85.2%; specificity, 85.3%; and AUC, 0.899). In both layers, the highest AUC was observed at 7 o'clock, except in the innermost circle. In the superficial layer, there were significant differences in AUCs at 7 o'clock between the innermost circle and the other outer circles (all $P < .05$). In the deep layer, all of the AUCs were less than 0.8, regardless of circle measurement location.

### Optimal region for vessel density measurement

In this study, the optimal region for the measurement of vessel density was determined to be the 2.7–5.5-mm-diameter circle, because the innermost circle showed eccentric features in spatial analysis and diagnostic ability. The AUCs of the vessel density of the optimal measurement region and the RNFL thickness are shown in Table 2. The superficial vessel density showed significantly better diagnostic performance than the deep vessel density in superior and inferior quadrants or at 11, 12, 1, 6, and 7 o'clock. On the other

**Table 1** Demographic and clinical characteristics of normal and glaucoma subjects

| | Healthy ($n$ = 51) | Glaucoma ($n$ = 42) | P |
|---|---|---|---|
| Age (years) | 50.7 ± 15.7 | 51.8 ± 14.2 | 0.642 |
| Gender (male:female) | 23:28 | 23:19 | 0.472 |
| Intraocular pressure (mmHg) | 14.3 ± 3.0 | 14.5 ± 3.8 | 0.746 |
| Refractive error (diopters) | −1.37 ± 2.41 | −2.53 ± 3.27 | 0.097 |
| Axial length (mm) | 24.0 ± 1.3 | 24.6 ± 1.9 | 0.152 |
| CCT (μm) | 544.2 ± 37.3 | 534.1 ± 39.1 | 0.213 |
| Visual field mean deviation (dB) | −0.97 ± 1.86 | −5.88 ± 6.01 | <0.001 |
| Average RNFL thickness (μm) | 95.2 ± 10.3 | 79.3 ± 11.0 | <0.001 |
| Disc area ($mm^2$) | 2.38 ± 0.51 | 2.27 ± 0.69 | 0.383 |

*CCT* central corneal thickness, *RNFL* retinal nerve fiber layer

**Table 2** Comparisons of area under receiver operating characteristic curve (AUC) of vessel density within the optimal measuring region and retinal nerve fiber layer thickness

| | Superficial layer Vessel Density | | | Deep layer Vessel Density | | | Retinal nerve fiber layer Thickness | | | P | | |
|---|---|---|---|---|---|---|---|---|---|---|---|---|
| | Healthy | Glaucoma | AUC (95% CI) (a) | Healthy | Glaucoma | AUC (95% CI) (b) | Healthy | Glaucoma | AUC (95% CI) (c) | a-b | a-c | b-c |
| Average | 58.9 ± 9.8 | 48.4 ± 9.8 | 0.775 (0.652–0.871) | 39.0 ± 9.4 | 33.4 ± 7.5 | 0.671 (0.542–0.785) | 95.2 ± 10.3 | 78.9 ± 11.7 | 0.841 (0.727–0.921) | 0.07 | 0.34 | 0.04 |
| | | | | | | Quadrant | | | | | | |
| Temporal | 61.0 ± 14.7 | 50.0 ± 15.7 | 0.706 (0.578–0.814) | 37.9 ± 16.6 | 28.3 ± 14.0 | 0.664 (0.534–0.778) | 70.5 ± 7.6 | 64.4 ± 12.4 | 0.678 (0.549–0.791) | 0.42 | 0.76 | 0.88 |
| Superior | 63.8 ± 9.1 | 51.0 ± 12.8 | 0.777 (0.654–0.872) | 36.2 ± 10.7 | 31.2 ± 9.4 | 0.627 (0.496–0.745) | 115.8 ± 15.3 | 96.4 ± 18.8 | 0.784 (0.663–0.878) | 0.03 | 0.91 | 0.11 |
| Nasal | 47.7 ± 13.2 | 46.0 ± 12.9 | 0.539 (0.408–0.665) | 40.2 ± 13.0 | 41.0 ± 13.4 | 0.522 (0.393–0.650) | 72.5 ± 14.9 | 66.0 ± 13.5 | 0.617 (0.486–0.737) | 0.91 | 0.46 | 0.37 |
| Inferior | 63.1 ± 10.6 | 46.5 ± 12.4 | 0.839 (0.724–0.919) | 41.9 ± 10.2 | 33.0 ± 9.1 | 0.743 (0.618–0.845) | 122.1 ± 15.0 | 88.4 ± 21.4 | 0.890 (0.786–0.955) | 0.04 | 0.40 | 0.04 |
| | | | | | | Clock-hour | | | | | | |
| 9 | 54.1 ± 16.9 | 48.6 ± 15.2 | 0.612 (0.480–0.732) | 39.1 ± 20.3 | 29.9 ± 17.2 | 0.643 (0.512–0.760) | 57.1 ± 6.9 | 56.8 ± 12.2 | 0.518 (0.388–0.646) | 0.57 | 0.39 | 0.24 |
| 10 | 68.3 ± 14.1 | 55.4 ± 18.1 | 0.714 (0.586–0.821) | 37.6 ± 16.9 | 26.6 ± 13.8 | 0.683 (0.553–0.794) | 82.3 ± 11.9 | 74.1 ± 17.7 | 0.644 (0.513–0.760) | 0.58 | 0.35 | 0.69 |
| 11 | 75.8 ± 11.7 | 55.0 ± 17.9 | 0.824 (0.707–0.908) | 42.6 ± 18.5 | 30.0 ± 13.3 | 0.704 (0.575–0.812) | 124.4 ± 21.2 | 95.1 ± 30.6 | 0.776 (0.653–0.871) | 0.04 | 0.41 | 0.41 |
| 12 | 57.4 ± 12.9 | 45.9 ± 14.2 | 0.708 (0.580–0.816) | 27.1 ± 13.1 | 24.3 ± 12.5 | 0.567 (0.436–0.691) | 116.4 ± 22.9 | 93.7 ± 22.3 | 0.759 (0.635–0.858) | 0.01 | 0.54 | 0.05 |
| 1 | 58.3 ± 9.6 | 52.2 ± 13.7 | 0.642 (0.511–0.759) | 38.9 ± 11.3 | 39.2 ± 12.1 | 0.507 (0.378–0.635) | 106.7 ± 18.9 | 97.0 ± 20.3 | 0.643 (0.512–0.760) | 0.03 | 0.99 | 0.18 |
| 2 | 53.2 ± 13.8 | 48.6 ± 13.7 | 0.609 (0.478–0.730) | 44.5 ± 13.5 | 42.1 ± 13.1 | 0.560 (0.429–0.685) | 85.1 ± 20.7 | 77.8 ± 21.3 | 0.591 (0.460–0.714) | 0.29 | 0.86 | 0.76 |
| 3 | 46.6 ± 14.8 | 47.7 ± 15.1 | 0.521 (0.392–0.649) | 41.0 ± 15.0 | 43.3 ± 16.0 | 0.530 (0.400–0.657) | 62.1 ± 16.8 | 57.4 ± 12.5 | 0.566 (0.435–0.690) | 0.80 | 0.68 | 0.75 |
| 4 | 43.3 ± 15.1 | 41.8 ± 14.4 | 0.519 (0.390–0.647) | 35.1 ± 16.1 | 37.7 ± 16.1 | 0.551 (0.420–0.676) | 69.9 ± 13.5 | 62.8 ± 13.8 | 0.645 (0.514–0.762) | 0.83 | 0.22 | 0.39 |
| 5 | 47.2 ± 17.4 | 42.4 ± 13.1 | 0.599 (0.468–0.721) | 32.1 ± 16.2 | 30.6 ± 10.5 | 0.517 (0.388–0.645) | 102.4 ± 19.2 | 82.8 ± 20.2 | 0.764 (0.640–0.862) | 0.09 | 0.03 | <0.01 |
| 6 | 61.4 ± 14.5 | 47.2 ± 13.4 | 0.765 (0.641–0.862) | 39.0 ± 14.6 | 32.1 ± 10.8 | 0.676 (0.547–0.789) | 128.7 ± 21.0 | 93.0 ± 25.2 | 0.855 (0.744–0.931) | 0.04 | 0.19 | 0.02 |
| 7 | 80.6 ± 7.5 | 50.1 ± 22.0 | 0.898 (0.795–0.960) | 54.5 ± 15.7 | 36.2 ± 16.8 | 0.789 (0.668–0.882) | 135.0 ± 18.0 | 89.1 ± 30.7 | 0.913 (0.815–0.969) | <0.01 | 0.79 | <0.01 |
| 8 | 60.5 ± 17.1 | 46.2 ± 20.0 | 0.718 (0.590–0.824) | 37.0 ± 16.7 | 28.3 ± 15.0 | 0.666 (0.536–0.780) | 72.6 ± 9.4 | 62.4 ± 18.3 | 0.728 (0.601–0.832) | 0.26 | 0.91 | 0.47 |

*AUCs were compared using the method of DeLong et al. [21]

*CI* confidence interval

hand, there were no significant differences in AUCs between the superficial vessel density and RNFL thickness, except in the 5 o'clock area.

### Factors associated with superficial and deep vessel density in glaucoma

In glaucoma subjects, the association between vessel density and various clinical factors was assessed by univariate and multivariate regression analyses (Table 3). A worse VF MD and thinner average RNFL thickness were significantly associated with a decreased superficial vessel density. A longer axial length was significantly associated with a decreased deep vessel density.

## Discussion

In this study, we found that peripapillary vessel density varied according to the measurement position. In particular, the innermost circle (2.0–2.7-mm diameter) showed significantly different vessel density characteristics than the outer circles (2.7–5.5-mm diameter). Although recent OCTA studies adopted peripapillary vessel density as a representative parameter for evaluating perfusion status, there is no established consensus for the proper measurement position. In previous studies, peripapillary vessel density was measured in 500-μm- [12], 700-μm- [13], and 750-μm-wide [15] elliptical annuli extending from the optic disc boundary. Wang et al. [22] measured peripapillary vessel density between two concentric circles with a diameter from 1.5 to 3.4 mm. The absence of a standardized measurement position might cause difficulties in comparisons of the peripapillary vessel density. Various regional analyses of vessel density could provide useful information to determine the appropriate measurement position for OCTA.

The optimal region (2.7–5.5-mm diameter circles) for measuring vessel density was determined by considering the (1) maximal inclusion of vascular information, (2) minimal influence of optic disc size, and (3) efficient diagnostic performance. Most previous OCTA studies focused on the microvasculature in the optic disc [23, 24] or the small region (3 × 3 mm or 4.5 × 4.5 mm) adjacent to the optic disc [12, 13, 15, 22]. The RPC runs along the paths of the major superotemporal and inferotemporal vessels 4–5 mm from the optic disc [7]. Yarmohammadi et al. [15] reported that a larger measurement area is better at detecting changes in the RPCs. Recent commercial OCTA devices provide microvascular flow images in a 6 × 6-mm region. To investigate the RPCs, we explored the vascular characteristics as much as possible around the optic disc.

The major blood vessels of the retina radiate from the ONH, and RPCs originate from retinal vessels around the optic disc [25, 26]. RPCs are the most superficial layer of capillaries lying in the inner part of the RNFL [7], and a close relationship between RPCs and RNFL was found in a recent OCTA study [17]. A histologic study showed that RNFL thickness decreases as the distance increases from the optic disc margin [27]. In this study, the superficial vessel density gradually decreased according to the distance from the optic disc margin. However, the innermost circle did not follow this trend and the diagnostic performance of the innermost circle was not as good as that of outer circles. The optic disc is quite variable in appearance and its size affects peripapillary structural measurements [28]. The eccentric features of innermost circle might be related to the variety of the optic disc. Therefore, the region adjacent to the optic disc margin was inappropriate for vessel density measurements.

In the present study, the peripapillary vessel density of glaucoma patients was decreased in both superficial and deep retinal layers. Loss of RPCs in the superficial retinal layer has been shown in previous OCTA studies [12, 13, 15].

**Table 3** Univariate and multivariate regression analysis to determine the factors associated with the vessel density in glaucoma subjects

| | Superficial vessel density | | | | Deep vessel density | | | |
|---|---|---|---|---|---|---|---|---|
| | Univariate | | Multivariate ($R^2$ = 0.299) | | Univariate | | Multivariate ($R^2$ = 0.227) | |
| | Coefficient (95% CI) | P | Coefficient (95% CI) | P | Coefficient (95% CI) | P | Coefficient (95% CI) | P |
| Age | −0.079 (−0.297; 0.139) | 0.468 | | | 0.057 (−0.152; 0.266) | 0.583 | | |
| IOP | -0.185 (−0.951; 0.580) | 0.628 | | | −0.338 (−1.065; −0.039) | 0.045 | −0.314 (−1.195; 0.566) | 0.169 |
| Axial length | −1.328 (−2.884; 0.229) | 0.091 | | | −1.613 (−2.871; −0.355) | 0.014 | −1.650 (−2.926; −0.374) | 0.013 |
| CCT | 0.007 (−0.070; 0.085) | 0.848 | | | −0.025 (−0.091; 0.040) | 0.437 | | |
| Disc area | 2.039 (−3.404; 7.482) | 0.451 | | | 3.445 (−1.748; 8.637) | 0.186 | | |
| VF MD | 0.653 (0.228; 1.078) | 0.003 | 0.733 (0.192; 1.274) | 0.013 | 0.219 (−0.225; 0.663) | 0.325 | | |
| RNFLT | 0.368 (0.030; 0.705) | 0.034 | 0.308 (0.012; 0.627) | 0.045 | 0.069 (−0.275; 0.413) | 0.686 | | |

*CI* confidence interval, *IOP* intraocular pressure, *CCT* central corneal thickness, *VF MD* visual field mean deviation, *RNFLT* retinal nerve fiber layer thickness

Interestingly, the deep capillary bed was also affected by the glaucomatous change, although the difference was subtle compared with that of RPCs in the superficial retinal layer [e.g., the difference in the average vessel density between healthy and glaucoma subjects: 10.5% (from 58.9% to 48.4%) in superficial vs. 5.6% (from 39.0% to 33.4%) in deep retinal layers; Table 2]. Because RPCs anastomose with deeper capillaries [7], an ischemic change in the superficial retinal layer might cause collateral damage in the deep retinal capillary plexus. When we interpreted the OCTA images, disruption of the capillary network was prominent in the superficial layer but was hard to distinguish clearly in the deep layer (Fig. 4). Quantification of the vessel density might help to identify subtle vascular changes.

The posterior ciliary artery is the main source of blood supply to the ONH and also supplies the choroid and the outer 130 μm of the retina [29]. Because of the end-arterial nature of the posterior ciliary arteries and their branches, watershed zones in choroidal circulation have been confirmed in several studies [29–32]. The watershed zone could contribute to vascular insufficiency in the ONH in glaucoma [29]. In this study, we found that the deep vascular density was extremely decreased as a wedge-shaped pattern at 12 and 5 o'clock in both healthy and glaucomatous eyes. The vertically elongated vessel deficiency around the optic disc resembles the distribution pattern of the choroidal watershed zone [29, 30]. This finding implies the possibility of the presence of a watershed zone in the deep retinal capillary network. Because the watershed zone is vulnerable to ischemia, further investigation is needed for deep vascular structure.

At 7 o'clock, where is the most susceptible area in glaucoma, AUC (0.898) of superficial vessel density appeared to be highest. In addition, the superficial vessel density showed similar AUCs for the detection of glaucoma compared with RNFL thickness. This finding is consistent with those of previous studies. Liu et al. [13] reported that there was no significant difference between the AUCs of vessel density (0.938) and RNFL thickness (0.970). Yarmohammadi et al. [13] compared circumpapillary and whole image vessel density (AUCs, 0.83 and 0.94, respectively) to RNFL thickness (AUCs, 0.92).

On the other hand, the deep vessel density (highest AUC, 0.789 at 7 o'clock) showed a worse diagnostic performance than the superficial vessel density and RNFL thickness. Recently, Mammo et al. [33] reported that deeper capillary networks appeared structurally normal in glaucomatous eyes while RPC loss were identified in superficial layer. Their findings could explain poor discriminating ability between normal and glaucomatous eyes in this study. However, it should be noted a poor diagnostic ability of deep vessel density could be simply caused by the interrupted signal intensity from a flow projection artifact. The visualization of deep retinal vasculature is disturbed by a flow projection artifact, which comes from fluctuating shadows cast by flowing blood cells in the more superficial vessels [34]. Many

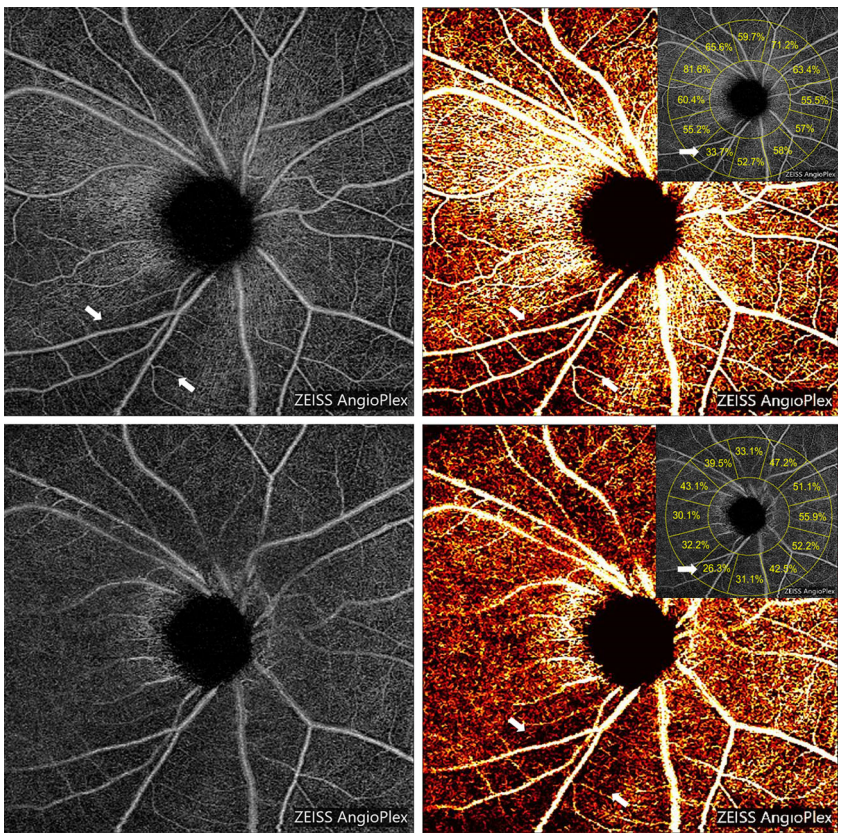


**Fig. 4** Peripapillary vessel density of glaucoma patients was decreased in both superficial and deep retinal layers. (Left column) In optical coherence tomography angiography image, the disruption of the capillary network (arrows) was prominent in the superficial layer, but it was hard to see clearly in the deep layer. (Right column) A multilevel threshold test enhanced the visibility of the vascular network in both superficial and deep layers. Quantification of the vessel density could assist to identify subtle vascular changes

attempts have been tried to minimize this problem, but removing projection artifacts are still in the development phase [34, 35].

Large-scale population-based studies have reported that myopia is a risk factor for glaucoma development [36–40]. Interestingly, axial length was correlated only with deep vessel density, although both superficial and deep vasculatures were reduced in glaucomatous eyes. Previous studies reported that the choroid, which is a vascular layer providing oxygen and nourishment to the outer retina, is decreased with myopia severity [41, 42]. These findings may imply that myopic changes mainly affect deeper circulation rather than superficial RPCs in glaucomatous eyes.

Our study has several limitations of note. The AUCs of average superficial vessel density and RNFL thickness were 0.775 and 0.841, respectively. These values were relatively lower compared to many previous reports with high AUCs more than 0.9 [13, 15, 43, 44]. However, the discrimination ability is dependent on the severity of glaucoma, with better performance in discriminating between healthy and more advanced disease compared with discrimination of early stages of glaucoma [43, 45]. Our study was composed of 71.4% early stage glaucoma and the results should be interpreted in this context. Second, according to previous publications [46, 47], most Korean open-angle glaucoma patients have a statistically normal range of IOP values and thus our current study focused in NTG patients. Hence, other ethnicities with different IOP profiles may have different outcomes. Third, because we used our customized program for detailed analysis, the outcome may have to be re-analyzed when manufacturer releases appropriate commercially available software. Finally, a cause and effect relationship between glaucoma pathogenesis and vascular factors could not be determined by this cross-sectional study and any such possible relationship should be confirmed in a future longitudinal study.

In conclusion, the vessel density maps provided spatial information on the peripapillary vessel distribution in healthy and glaucomatous eyes. Our results offer clues for the optimal area for the measurement of peripapillary vessel density. Although both superficial and deep vasculatures were reduced in glaucomatous eyes, only the superficial vascular layer showed comparable diagnostic performance in the diagnosis of glaucoma. The deep layer was affected by axial length and did not show a relationship with glaucoma severity. Understanding of the characteristics of vasculature at various spatial locations and layers may be helpful in clinical practice and further research.

#### Compliance with ethical standards

**Funding** No funding was received for this research.

**Conflict of interest** All authors certify that they have no affiliations with or involvement in any organization or entity with any financial interest (such as honoraria; educational grants; participation in speakers' bureaus; membership, employment, consultancies, stock ownership, or other equity interest; and expert testimony or patent-licensing arrangements), or non-financial interest (such as personal or professional relationships, affiliations, knowledge or beliefs) in the subject matter or materials discussed in this manuscript.

**Ethical approval** All procedures performed in studies involving human participants were in accordance with the ethical standards of the institutional and/or national research committee and with the 1964 Helsinki declaration and its later amendments or comparable ethical standards.

**Informed consent** Informed consent was obtained from all individual participants included in the study.

## References

1. Flammer J, Orgul S, Costa VP, Orzalesi N, Krieglstein GK, Serra LM, Renard JP, Stefansson E (2002) The impact of ocular blood flow in glaucoma. Prog Retin Eye Res 21:359–393
2. Chung HS, Harris A, Kagemann L, Martin B (1999) Peripapillary retinal blood flow in normal tension glaucoma. Br J Ophthalmol 83: 466–469
3. Harris A, Sergott RC, Spaeth GL, Katz JL, Shoemaker JA, Martin BJ (1994) Color Doppler analysis of ocular vessel blood velocity in normal-tension glaucoma. Am J Ophthalmol 118:642–649
4. Mitchell P, Leung H, Wang JJ, Rochtchina E, Lee AJ, Wong TY, Klein R (2005) Retinal vessel diameter and open-angle glaucoma: the Blue Mountains eye study. Ophthalmology 112:245–250
5. Wang S, Xu L, Wang Y, Wang Y, Jonas JB (2007) Retinal vessel diameter in normal and glaucomatous eyes: the Beijing eye study. Clin Experiment Ophthalmol 35:800–807
6. Yu DY, Cringle SJ, Balaratnasingam C, Morgan WH, Yu PK, Su EN (2013) Retinal ganglion cells: energetics, compartmentation, axonal transport, cytoskeletons and vulnerability. Prog Retin Eye Res 36:217–246
7. Zhang HR (1994) Scanning electron-microscopic study of corrosion casts on retinal and choroidal angioarchitecture in man and animals. Prog Retin Eye Res 13:243–270
8. Alterman M, Henkind P (1968) Radial peripapillary capillaries of the retina. II. Possible role in Bjerrum scotoma. Br J Ophthalmol 52:26–31
9. Kornzweig AL, Eliasoph I, Feldstein M (1968) Selective atrophy of the radial peripapillary capillaries in chronic glaucoma. Arch Ophthalmol 80:696–702
10. Spaide RF, Klancnik JM Jr, Cooney MJ (2015) Retinal vascular layers imaged by fluorescein angiography and optical coherence tomography angiography. JAMA Ophthalmol 133:45–50
11. Mendis KR, Balaratnasingam C, Yu P, Barry CJ, McAllister IL, Cringle SJ, Yu DY (2010) Correlation of histologic and clinical images to determine the diagnostic value of fluorescein angiography for studying retinal capillary detail. Invest Ophthalmol Vis Sci 51:5864–5869
12. Akagi T, Iida Y, Nakanishi H, Terada N, Morooka S, Yamada H, Hasegawa T, Yokota S, Yoshikawa M, Yoshimura N (2016) Microvascular density in glaucomatous eyes with Hemifield visual field defects: an optical coherence tomography angiography study. Am J Ophthalmol 168:237–249
13. Liu L, Jia Y, Takusagawa HL, Pechauer AD, Edmunds B, Lombardi L, Davis E, Morrison JC, Huang D (2015) Optical coherence tomography angiography of the Peripapillary retina in glaucoma. JAMA Ophthalmol 133:1045–1052
14. Bojikian KD, Chen CL, Wen JC, Zhang Q, Xin C, Gupta D, Mudumbai RC, Johnstone MA, Wang RK, Chen PP (2016) Optic disc perfusion in primary open angle and normal tension glaucoma

eyes using optical coherence tomography-based Microangiography. PLoS One 11:e0154691
15. Yarmohammadi A, Zangwill LM, Diniz-Filho A, Suh MH, Manalastas PI, Fatehee N, Yousefi S, Belghith A, Saunders LJ, Medeiros FA, Huang D, Weinreb RN (2016) Optical coherence tomography angiography vessel density in healthy, glaucoma suspect, and glaucoma eyes. Invest Ophthalmol Vis Sci 57:451–459
16. Hollo G (2016) Vessel density calculated from OCT angiography in 3 peripapillary sectors in normal, ocular hypertensive, and glaucoma eyes. Eur J Ophthalmol 26:e42–e45
17. Yu PK, Cringle SJ, Yu DY (2014) Correlation between the radial peripapillary capillaries and the retinal nerve fibre layer in the normal human retina. Exp Eye Res 129:83–92
18. An L, Johnstone M, Wang RK (2012) Optical microangiography provides correlation between microstructure and microvasculature of optic nerve head in human subjects. J Biomed Opt 17:116018
19. Zhang A, Zhang Q, Chen CL, Wang RK (2015) Methods and algorithms for optical coherence tomography-based angiography: a review and comparison. J Biomed Opt 20:100901
20. Shahlaee A, Samara WA, Hsu J, Say EA, Khan MA, Sridhar J, Hong BK, Shields CL, Ho AC (2016) In vivo assessment of macular vascular density in healthy human eyes using optical coherence tomography angiography. Am J Ophthalmol 165:39–46
21. DeLong ER, DeLong DM, Clarke-Pearson DL (1988) Comparing the areas under two or more correlated receiver operating characteristic curves: a nonparametric approach. Biometrics 44:837–845
22. Wang Q, Chan S, Yang JY, You B, Wang YX, Jonas JB, Wei WB (2016) Vascular density in retina and choriocapillaris as measured by optical coherence tomography angiography. Am J Ophthalmol
23. Jia Y, Wei E, Wang X, Zhang X, Morrison JC, Parikh M, Lombardi LH, Gattey DM, Armour RL, Edmunds B, Kraus MF, Fujimoto JG, Huang D (2014) Optical coherence tomography angiography of optic disc perfusion in glaucoma. Ophthalmology 121:1322–1332
24. Wang X, Jiang C, Ko T, Kong X, Yu X, Min W, Shi G, Sun X (2015) Correlation between optic disc perfusion and glaucomatous severity in patients with open-angle glaucoma: an optical coherence tomography angiography study. Graefes Arch Clin Exp Ophthalmol 253:1557–1564
25. Henkind P (1967) Radial peripapillary capillaries of the retina. I. Anatomy: human and comparative. Br J Ophthalmol 51:115–123
26. Scoles D, Gray DC, Hunter JJ, Wolfe R, Gee BP, Geng Y, Masella BD, Libby RT, Russell S, Williams DR, Merigan WH (2009) In-vivo imaging of retinal nerve fiber layer vasculature: imaging histology comparison. BMC Ophthalmol 9:9
27. Garcia-Valenzuela E, Mori M, Edward DP, Shahidi M (2000) Thickness of the peripapillary retina in healthy subjects with different degrees of ametropia. Ophthalmology 107:1321–1327
28. Budenz DL, Anderson DR, Varma R, Schuman J, Cantor L, Savell J, Greenfield DS, Patella VM, Quigley HA, Tielsch J (2007) Determinants of normal retinal nerve fiber layer thickness measured by stratus OCT. Ophthalmology 114:1046–1052
29. Hayreh SS (2004) Posterior ciliary artery circulation in health and disease: the Weisenfeld lecture. Invest Ophthalmol Vis Sci 45:749–757 **748**
30. Hayreh SS (1990) In vivo choroidal circulation and its watershed zones. Eye (Lond) 4(Pt 2):273–289
31. Ross RD, Barofsky JM, Cohen G, Baber WB, Palao SW, Gitter KA (1998) Presumed macular choroidal watershed vascular filling, choroidal neovascularization, and systemic vascular disease in patients with age-related macular degeneration. Am J Ophthalmol 125:71–80
32. Takahashi K, Muraoka K, Kishi S, Shimizu K (1996) Watershed zone in the human peripheral choroid. Ophthalmology 103:336–342
33. Mammo Z, Heisler M, Balaratnasingam C, Lee S, Yu DY, Mackenzie P, Schendel S, Merkur A, Kirker A, Albiani D, Navajas E, Beg MF, Morgan W, Sarunic MV (2016) Quantitative optical coherence tomography angiography of radial Peripapillary capillaries in glaucoma, glaucoma suspect, and normal eyes. Am J Ophthalmol 170:41–49
34. Zhang M, Hwang TS, Campbell JP, Bailey ST, Wilson DJ, Huang D, Jia Y (2016) Projection-resolved optical coherence tomographic angiography. Biomed Opt Express 7:816–828
35. Zhang A, Zhang Q, Wang RK (2015) Minimizing projection artifacts for accurate presentation of choroidal neovascularization in OCT micro-angiography. Biomed Opt Express 6:4130–4143
36. Mitchell P, Hourihan F, Sandbach J, Wang JJ (1999) The relationship between glaucoma and myopia: the Blue Mountains eye study. Ophthalmology 106:2010–2015
37. Perera SA, Wong TY, Tay WT, Foster PJ, Saw SM, Aung T (2010) Refractive error, axial dimensions, and primary open-angle glaucoma: the Singapore Malay eye study. Arch Ophthalmol 128:900–905
38. Sommer A, Tielsch JM (1996) Risk factors for open-angle glaucoma: the Barbados eye study. Arch Ophthalmol 114:235
39. Wong TY, Klein BE, Klein R, Knudtson M, Lee KE (2003) Refractive errors, intraocular pressure, and glaucoma in a white population. Ophthalmology 110:211–217
40. Xu L, Wang Y, Wang S, Wang Y, Jonas JB (2007) High myopia and glaucoma susceptibility the Beijing eye study. Ophthalmology 114:216–220
41. Shin JW, Shin YU, Lee BR (2012) Choroidal thickness and volume mapping by a six radial scan protocol on spectral-domain optical coherence tomography. Ophthalmology 119:1017–1023
42. Ho M, Liu DT, Chan VC, Lam DS (2013) Choroidal thickness measurement in myopic eyes by enhanced depth optical coherence tomography. Ophthalmology 120:1909–1914
43. Bussel II, Wollstein G, Schuman JS (2014) OCT for glaucoma diagnosis, screening and detection of glaucoma progression. Br J Ophthalmol 98(Suppl 2):ii15-19
44. Mwanza JC, Oakley JD, Budenz DL, Anderson DR (2011) Ability of cirrus HD-OCT optic nerve head parameters to discriminate normal from glaucomatous eyes. Ophthalmology 118(241–248):e241
45. Bengtsson B, Andersson S, Heijl A (2012) Performance of time-domain and spectral-domain optical coherence tomography for glaucoma screening. Acta Ophthalmol 90:310–315
46. Kim CS, Seong GJ, Lee NH, Song KC, Namil Study Group KGS (2011) Prevalence of primary open-angle glaucoma in central South Korea the Namil study. Ophthalmology 118:1024–1030
47. Suh W, Kee C, Namil Study G, Korean Glaucoma S (2012) The distribution of intraocular pressure in urban and in rural populations: the Namil study in South Korea. Am J Ophthalmol 154:99–106